URSI - RCRS 2022, IIT (Indore), India, 1 - 4 December, 2022

Characterization of ITCZ using deep convective cloud cores derived using the water vapour absorption channels around 183.31 GHz onboard SAPHIR/Megha-Tropiques

Sisma Samuel*(1,2), Nizy Mathew (1), and V. Sathiyamoorthy(1)
(1) Space Physics Laboratory, Vikram Sarabhai Space Centre, Thiruvananthapuram-695022, India.
(2) Faculty of Science, Cochin University of Science and Technology, Kochi-682022, India.

Abstract

The intertropical convergence zone (ITCZ) is a region encircling the globe near the equator where the surface trade winds of both the hemispheres meet. It is characterized by deep convective clouds and accounts for more than 30% of global precipitation. Conventionally, parameters such as low outgoing longwave radiation (OLR), high precipitation and strong surface wind convergence (SWC) are used to identify and characterize the ITCZ. These parameters suffer from some inherent issues while identifying ITCZ. A new method based on the identification of deep convective cloud cores (DCCCs), derived from brightness temperature (T_B) data of the water vapor absorption channels of Sondeur Atmosphérique du Profil d'Humidité Intertropicale par Radiométrie (SAPHIR), aboard Megha-Tropiques (MT) satellite is proposed in this work. The present method identifies the DCCCs and performs better over (a) anvils and cirrus-dominated areas where OLR-based methods face difficulties, (b) coastal and continental areas where satellite scatterometer data are unavailable to estimate surface convergence and (c) windward side of orographic regions where rainfall based methods fail. The global mean position of ITCZ is north of the equator, with maximum northward migration up to 24ºN during June-August over the Asian summer monsoon region and maximum southward migration up to 20ºS during December-February over the Indian and the Pacific Oceans, respectively.

1. Introduction

The intertropical convergence zone (ITCZ) is a longitudinally oriented belt of convergence and associated convection over the globe in the near-equatorial region, accounting for more than 30% of global precipitation. ITCZ is a low-pressure region near the equator where surface northeasterly trade winds from the northern hemisphere and south-easterly trade winds from the southern hemisphere meet [1]. It is characterized by maximum precipitation, zero meridional mass-momentum flux, low-level wind convergence, strong vertical motion, and high occurrence of deep convective clouds (DCCs) [2]–[8]. The convective cloud cores associated with ITCZ significantly transport energy, mass, and momentum vertically and horizontally. They drive the Hadley and Walker circulations and influence both the radiation budget and the hydrological cycle [2], [9]–[11]. The enhanced cloudiness associated with ITCZ provides a significant contribution to planetary albedo. The ITCZ could influence global temperature, precipitation and climate change through the influence on the global radiation budget [12]–[14]. Therefore, it is essential to understand the characteristics of ITCZ, such as the strength, position, north-south migration, and variability in different timescales. Several of the earlier studies have been devoted to understanding various aspects of ITCZ, such as structure, strength, variability, dynamics, role on atmospheric energy transport and association with Sea Surface Temperature (SST).

Traditionally, parameters such as maximum rainfall, minimum Outgoing Longwave Radiation (OLR), and surface wind convergence (SWC) are used to identify the ITCZ [1], [3], [5], [8], [15]–[18]. Due to the complex land/sea distributions, the characteristics of ITCZ over different regions of the tropics are different. The annual mean position of ITCZ is north of the equator. Previous studies using modeling and observations have shown that the strength of the ITCZ is directly proportional to the inter-hemispheric energy gradient, cross-equatorial energy transport and inversely proportional to the strength of the zonal mean energy flux across the equator [5], [19], [20]. Similarly, modern coupled general circulation models (GCMs) suffer from the so-called dITCZ problem, i.e., high precipitation counterpart in the Southern Hemisphere (SH) corresponding to the strong Northern Hemisphere (NH) precipitation band, making the representation of the exact position of the ITCZ a challenge [21]–[23]. Despite the availability of several methods for detecting ITCZ, some discrepancies still exist over continents, where the trade winds are not well developed [1].

Conventionally, methods for identifying ITCZ are based on minimum thresholds of the satellite infrared brightness temperature (IR-BT), minimum OLR, high precipitation or strong SWC. IR-BT and OLR data from satellites identify the DCCs with cold cloud tops that will form as a result of surface wind convergence from both hemispheres. This method identifies high-level cirrus, cirrostratus and cirrocumulus cloud fractions with cold temperatures associated with deep convective events, also as deep convective clouds. From the scatterometer data over the global oceans, the occurrence of convergence near the surface can be derived, and it does not infer whether it will lead to deep convection. Satellite-based IR measurements infer rainfall indirectly from cloud top temperatures which may fail over cloud anvil regions. Also, rainfall-based ITCZ classification fails over strong orographic and stratiform rainfall regions. Convective rain occurs along with stratiform rain over the tropics, and the latter is more pronounced over land than the ocean. Therefore, the ITCZ identified using precipitation data can be broader. Also, the narrow swath and the long revisit time of four to five days of satellite precipitation RADARs make monitoring of short-lived convective precipitation/clouds a challenge. In the present study, deep convective cloud cores (DCCCs), where the upscale growth of the cloud system occurs, alone are detected without the associated anvils, using passive microwave-sounding channel measurements by Sondeur Atmosphrique du Profil d'Humidité Intertropicale par Radiométrie (SAPHIR) aboard the low-inclination satellite Megha-Tropiques (MT). The SAPHIR payload channels near the water vapor absorption line centered at 183.31 GHz are used to identify DCCCs. The frequencies farther from the center can penetrate deeper into the clouds, and hence larger is the brightness temperature (T_B) depression in the presence of DCCCs. The criteria based on T_B difference between the channels can discern DCCC better than infrared satellite data, which misinterprets convective anvils also as DCCC [24]–[27].

The objective of the present work is to study the strength, variability, and north-south extent of ITCZ based on the occurrence frequency of DCCCs (OFD) estimated from SAPHIR T_B data. The mean position and migration of ITCZ using DCCCs derived from passive microwave sounder is studied for the first time. The advantage of the present method over the other conventional methods will be demonstrated by comparing it with the ITCZ derived using precipitation, OLR and SWC from different satellite observations. The factors affecting convection, such as SST, SWC, dynamics and the evolutionary structure of double-ITCZ will be examined using the OFD. The relationship between underlying SST and surface wind fields will be examined. The study will help to accurately identify ITCZ and hence will be beneficial for validating GCMs. The paper is organized as follows: Section 2 describes the data and method of analysis, Section 3 describes the advantage of the present method in comparison to other methods and interannual variability of ITCZ, and the summary of results is given in Section 5.

2. Data and Methodology

2.1. Delineation of deep convective cloud cores from MT-SAPHIR T_B

MT is a collaborative satellite mission between the Center National d'Etudes Spatiales, France and the Indian Space Research Organization, and was launched on 11 October 2011 with the primary objective of studying atmospheric water vapor and energy budget parameters in the tropical region [28].The MT has an equatorially inclined orbit of ~20^o, which provides measurements over the tropics at different local times, unlike sun-synchronous polar-orbiting satellites. SAPHIR payload aboard MT has a swath of ~2060 km and a footprint size of 10 km at nadir. The present study makes use of the SAPHIR T_B (level 1-A1) data. Using the channels 183.31 ± 0.2 GHz (S_1), 183.31 ± 1.1 GHz (S_2), 183.31 ± 2.8 GHz (S_3), 183.31 ± 4.2 GHz (S_4), and 183.31 ± 6.8 GHz (S_5) of SAPHIR, a methodology has already been developed to detect convective clouds [26], [29] and the channel 183.31 ± 11.0 GHz (S_6) is not considered here since the surface emission contribution is significantly high in the brightness temperature measurement. The higher microwave frequencies close to 183.31 GHz are sensitive to scattering from precipitating and non-precipitating hydrometeors. In case of clear sky conditions,

$$T_{B6} > T_{B4} > T_{B3} > T_{B2} > T_{B1} \quad (1)$$

where T_{B5} , T_{B4} , etc. are the T_B measured at channels S_5 , S_4 , etc. The channels far from 183.31 GHz can see deeper into the atmosphere, where they detect higher temperatures during clear sky conditions. However, when the atmosphere becomes optically thicker, brightness temperature depression increases. The channel farthest from 183.31 GHz has the largest depression. Hence, the condition reverses in the case of deep convective clouds. This behavior is due to the different weighting functions of these channels. The frequency farthest from the peak absorption can see deeper into the clouds. [24]–[26]. The pixels with $T_{B1} \leq 235$ K are only considered for the analysis. Conditions for the identification of DCCC are:

$$T_{B,2} - T_{B,5} \geq T_D, T_{B,2} - T_{B,4} \geq T_D, T_{B,2} - T_{B,3} \geq T_D, T_{B,3} - T_{B,5} \geq T_D, \; T_{B,3} - T_{B,4} \geq T_D, T_{B,4} - T_{B,5} \geq T_D \quad (2)$$

where $T_{B,\alpha} - T_{B,\beta}$ is the difference in $T_{B(S\alpha)}$ and $T_{B(S\beta)}$ and α and β are the channel numbers for each observation of T_B with α < β. T_D is the incident angle-dependent threshold [25].

2.2 Ancillary Datasets

The present study utilizes the daily SWC data derived from the surface wind observations using the space-borne scatterometers aboard the Meteorological Operational (MetOp) satellite. Advanced Scatterometer (ASCAT-B) operates in the C-band (5.3-GHz). The broadband OLR is estimated from Scanner for Radiation Budget (ScaRaB) aboard the MT satellite. MT-ScaRaB can make measurements between ±30° latitudes over the tropics because of its wide swath of ~2200 km. ScaRaB measures radiance in 4 wavelength bands (i) Visible (0.55-0.65μm) (ii) Shortwave (0.2-4.0μm) (iii) Total (0.2-100μm) and (iv) Infrared (10.5-12.5μm) at all local times during the 51 day precession cycle. The Tropical Rainfall Measuring Mission (TRMM) 3B43 Version-6 precipitation data is used in this study. It is a combined product of satellite microwave imager and rain gauge observations. The vertical structure of clouds is obtained from the Cloud Profiling Radar (CPR) aboard the sun-synchronous polar-orbiting satellite CloudSat. It provides the altitude profiles of backscattered radar signals from hydrometeors at 94 GHz, with a vertical resolution of 240 m. The SST data is obtained from the Moderate Resolution Imaging Spectroradiometer (MODIS) onboard Aqua and Terra satellites.

3. Results

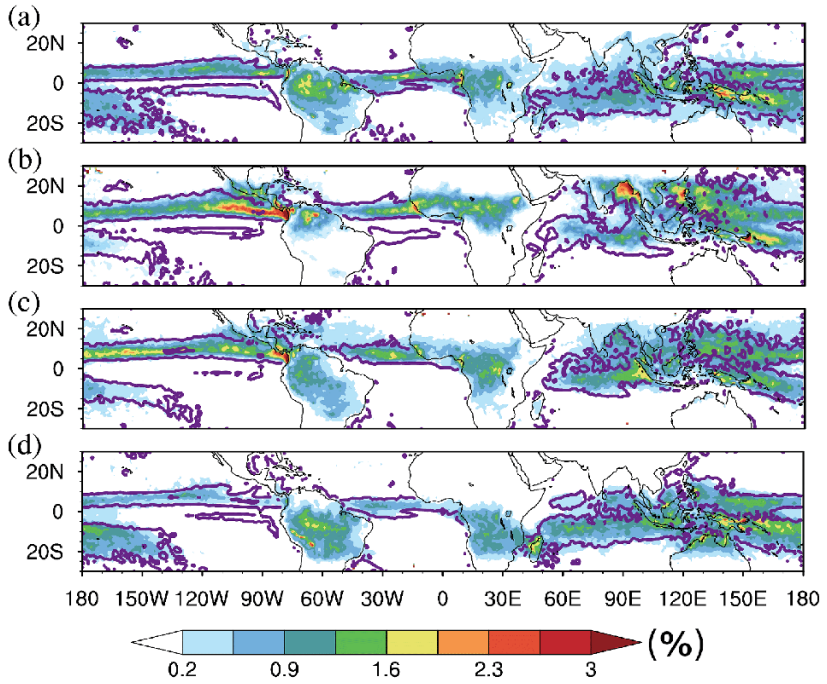

Figure 1. (a-d) Seasonal mean distribution of OFD (%) showing the width of ITCZ, the contours overlaid show the boundary of surface wind convergence threshold of $-0.1\times10^{-5}s^{-1}$ obtained from ASCAT measurements over the global oceans for MAM, JJA SON, and DJF for the period 2011-2018.

To identify the spatial extent and strength of ITCZ with better accuracy, OFD derived using the brightness temperature measurements of water vapor channels of SAPHIR is examined. Using T_B difference technique, DCCCs are identified over each pixel using the equations provided in Section 2.1. The OFD is calculated at each grid by using the following relation:

$$OFD = \frac{N_{DCCC}}{N_T} \quad (3)$$

where, N_{DCCC} is the number of observations identified as DCCC and N_T is the total number of observations. OFD is expressed in percentage [26], [27]. The monthly mean OFD is computed in a 1°× 1° geographical grid.

Figure 1 shows the distribution of mean OFD over the tropics for the four seasons along with SWC threshold of -0.1×10^{-5} s^{-1} and captures the characteristic features of ITCZ during different seasons. ITCZ identified by OFD is narrower than those identified by OLR and precipitation over the entire tropics (not shown). OFD distribution closely matches with the SWC

threshold except over the southern dITCZ over the east Pacific Ocean. The OFDs can also be used as a proxy for ITCZ over land where the scatterometer-based surface wind data is unavailable. Cirrus contamination and stratiform precipitation in OLR and rainfall data are greatly reduced in the ITCZ identified by OFD (not shown). The ITCZ is identified over the region where OFD is greater than 0.2% on a seasonal scale and eliminates scattered/unorganized convection.

In Figure 1 (a-d), ITCZ broadens and reaches up to 20°N over the Pacific Ocean during JJA. Over the Atlantic Ocean, the ITCZ migrates to 10°N in summer and 2°S in winter. The seasonal migration of ITCZ from the northern hemisphere to the southern hemisphere (summer to winter) is in concurrence with the movement of sun as observed from the four panels of Figure 1. Similar characteristics of ITCZ is evident when convective precipitation alone from the TRMM satellite is analyzed. The TRMM shows that convective precipitation is mainly distributed over the ITCZ, SPCZ, Asian summer monsoon region, south and central America and tropical Africa, with occurrence frequency between 1-2%. The spatial distribution of ITCZ identified from DCCC is closely matching with the spatial pattern obtained using convective precipitation from TRMM. The ITCZ is concentrated over the NH during MAM and JJA and migrates to SH during SON and DJF. The mean position of ITCZ is north of the equator over the Atlantic and the east Pacific Oceans. The maximum OFD reaches up to 4% over the Neotropics and the north Bay of Bengal during boreal summer. The OLR minimum reaches as low as 140 Wm^{-2} and the intensity of precipitation reaches up to 22 mm/day over the Neotropics. The South Pacific Convergence Zone (SPCZ) merges with the ITCZ over the western Pacific Ocean and aligns northwest to southeast across the southwest Pacific. It is more prominent during DJF and MAM than in the other two seasons. A dITCZ structure is found over the east Pacific Ocean during MAM with northern ITCZ between 3°N and 9°N and the southern counterpart between 2°S and 7°S with an occurrence frequency of around 0.3% or more and average precipitation of 4 mm/day. The dITCZ is often accompanied by off-equatorial SST maxima > 28°C with SST between 26°C and 27°C over the equator (not shown). Similarly, during DJF a double band structure of ITCZ is evident over the equatorial Indian Ocean, which starts appearing by November and disappears by January. The descending limb of Walker circulation over the Arabian sea is mostly devoid of deep convective clouds throughout the year, even on the tropical belt right over the equator. The intensities of precipitation and OFD are higher in South America compared to African landmass. However, over Africa, ITCZ exhibits large north-south migration compared to America. Parts of the Australian mainland are also associated with deep convective events during DJF with OFD of 1.4% and precipitation reaching up to 4 mm/day.

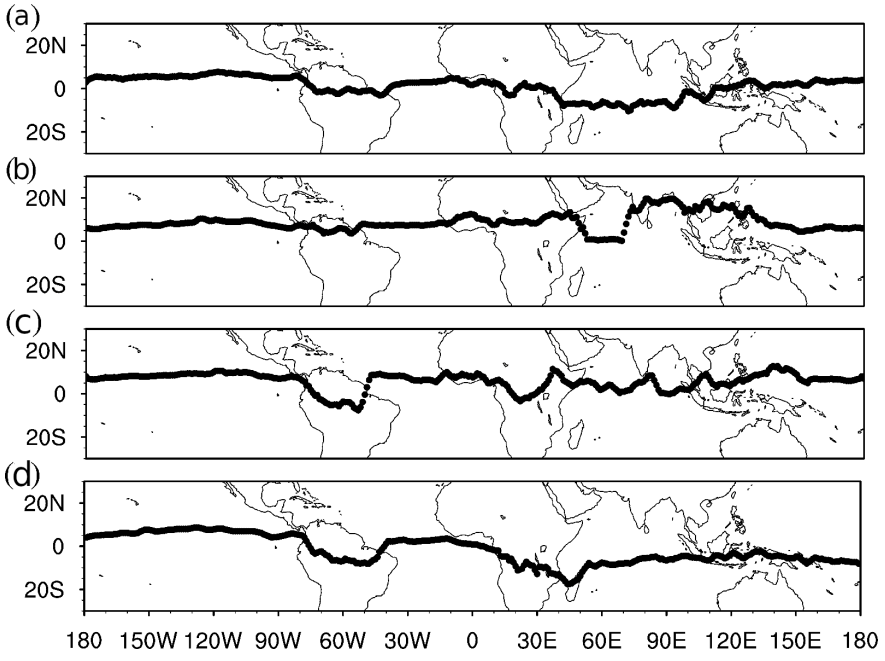

Figure 2. (a-d) the mean position of ITCZ based on the mean location of maximum OFD for MAM, JJA SON, and DJF for the period 2011-2018.

Figure 2 (a-d), shows the mean position of ITCZ based on the mean location of maximum OFD for 2011-2018. The mean position of ITCZ at every longitude is defined as the maximum time-mean OFD for each season that complies inside the region with SWC below the threshold of -0.1×10^{-5} s^{-1}. The southern dITCZ band is weaker than the northern band of ITCZ over the east Pacific Ocean. The band with the highest OFD is considered for identifying the mean position of ITCZ over the regions with double ITCZ. In Figure 2 (a-d), the seasonal migration of the mean position of ITCZ is evident. The migration is

less prominent over the east Pacific and Atlantic Oceans. The migration is more prominent in land regions compared to the ocean. The prominent migration of ITCZ occurs over the Indian Summer Monsoon region, where the mean position of ITCZ extends up to 24°N during JJA. The maximum southward migration occurs over the south Indian ocean, where the mean position of maximum OFD extends up to 19°S over Madagascar. The DCCCs and SWC above a threshold of 0.2% and -0.1×10^{-5} s^{-1}, respectively, show the width of ITCZ (Figure 1), and the mean location of maximum OFD shows the mean position of ITCZ (Figure 2) over the tropics for all seasons.

A detailed comparison of ITCZ derived using the four parameters OLR, OFD, precipitation and SWC are analyzed to bring out the advantages of the DCCC-based ITCZ identification. To demonstrate the strength of SAPHIR data in identifying DCCC, a case study of a tropical cyclone (Cyclone Imelda; 14 April 2013; 18°S to 22°S and 56°E to 62°E) that occurred over the South Indian Ocean is considered [31]. Figure 3 (a) shows the spatial map of SAPHIR T_B of Channel-S_5 overlaid with the track of CloudSat over Cyclone Imelda. The CloudSat RADAR reflectivity image of the tropical cyclone is shown in Figure 3 (b). The blue symbols overlaid over the cloud band represent the DCCC pixels identified by SAPHIR in this convective system, derived from collocated (within ± 10 km) and concurrent (within 1 h) SAPHIR measurements with the CloudSat observations. Figure 3 (c) shows the collocated and concurrent OLR derived from ScaRaB payload aboard MT for the same convective system. Figure 3 (d) shows the concurrent TRMM surface precipitation (average for 3 hrs). By comparing panels of Figure 3 (a)-(c) it is clear that OLR is unable to differentiate convective cores from thick cirrus anvils. The DCCC identified by SAPHIR T_B is a better indicator of convective core and avoids the anvil region.

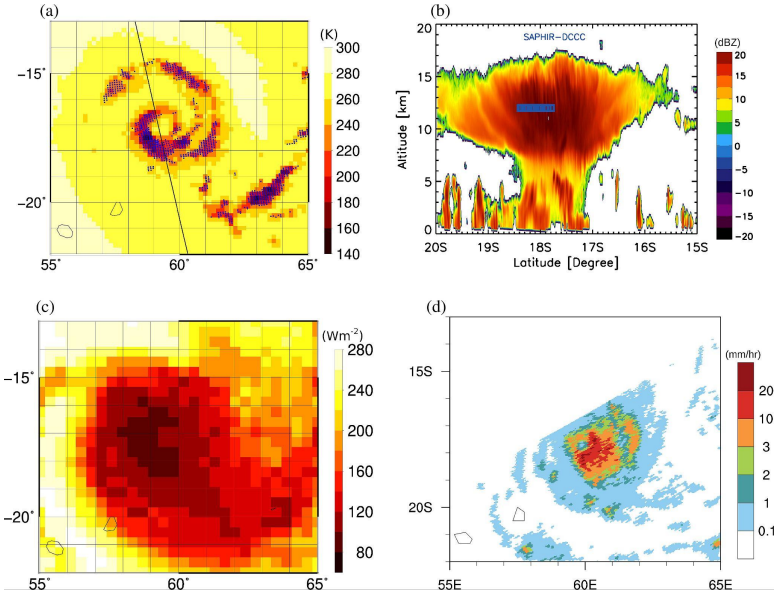

Figure 3. (a) SAPHIR T_B of channel S_5 overlaid with Cloudsat swath (black line) and DCCC (blue dots) (b) CloudSat RADAR reflectivity image of a convective system overlaid with collocated and concurrent SAPHIR identified DCCC (within 1 hr). (c) Collocated and concurrent OLR derived from ScaRaB (d) TRMM surface precipitation for the same convective system (average for 3 hrs).

Figure 4 shows the seasonal average OLR, SWC, precipitation, OFD for June-August 2012 over the Indian monsoon region located on the west coast of India. The spatial distribution of precipitation shows enormous rainfall on the windward side of the Western Ghats. The rainfall-based ITCZ identification method classifies this region as ITCZ formed by the convergence of winds from both hemispheres. However, this copious rainfall is not due to ITCZ but due to the orographic lifting of monsoon winds. Precipitation systems on the west coast of India are shallow in nature [32]. However, OFD data does not show any significant deep convective clouds over the west coast of India, and hence, the present methodology clearly delineates ITCZ from shallow orographic clouds. Rainfall-based ITCZ classification fails to delineate between heavy orographic precipitation and deep convective precipitation.

Figure 5 shows the seasonal average (a) OLR (b) SWC (c) precipitation and (d) OFD for the period of June-August 2012 over the east Pacific Ocean. In SWC the dITCZ structure exists over this region from June to August. However, precipitation, OLR, and DCCC data do not show a dITCZ structure. Though the SWC is more over the southern and northern dITCZ, heavy rainfall, low OLR and high OFD are seen over the northern hemispheric dITCZ and not over the southern hemispheric dITCZ. So the present method captures this difference in the deep convective cloud occurrence associated with southern and northern ITCZ clearly. Due to the added advantage of the present methodology in delineating ITCZ over other existing

methodologies on certain occasions, OFD is used for the detailed study of the monthly mean position of ITCZ over the tropics.

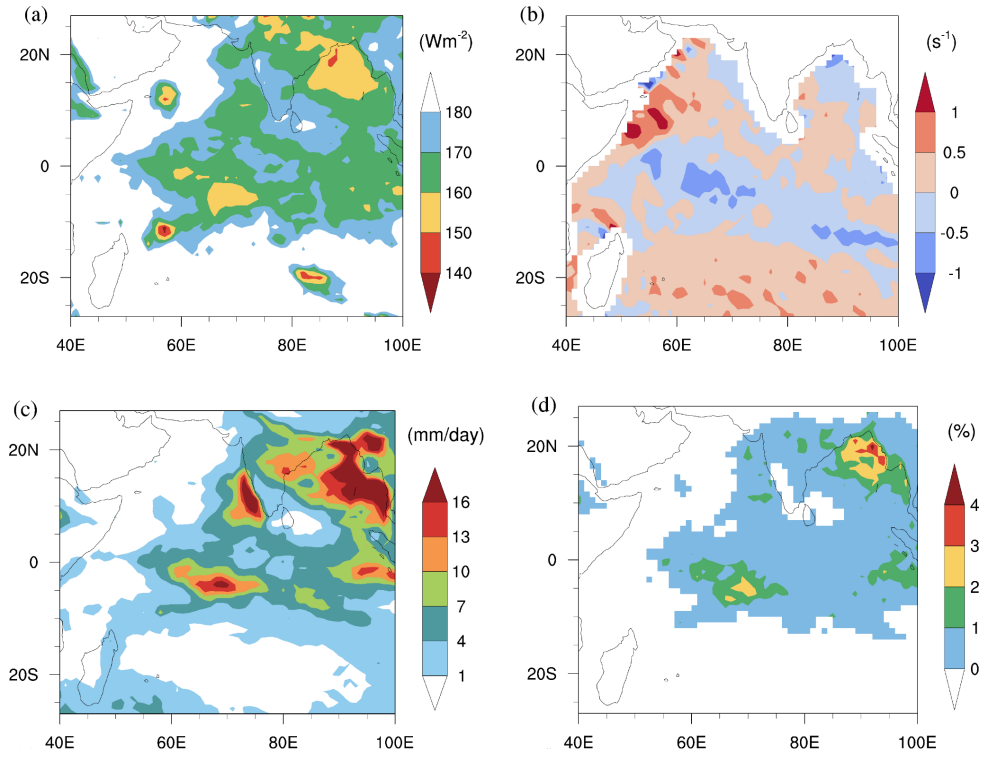

Figure 4. (a) OLR from ScaRaB (b) SWC from ASCAT (c) TRMM surface precipitation (d) DCCC from SAPHIR for the period June-August 2012 over the Indian subcontinent.

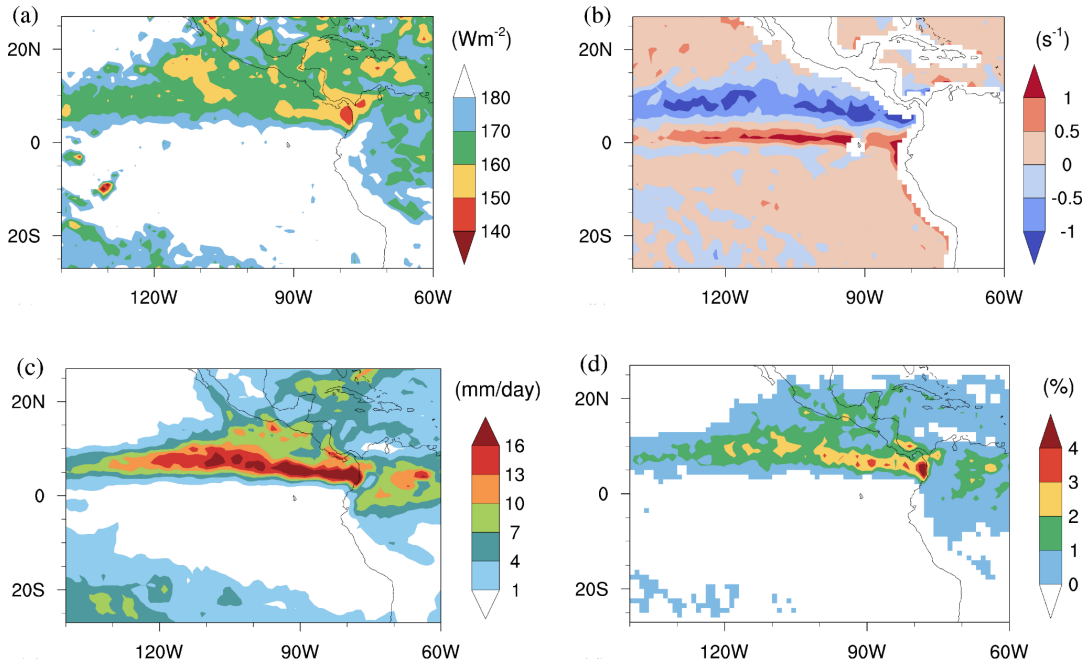

Figure 5. (a) OLR from ScaRaB (b) SWC from ASCAT (c) TRMM surface precipitation (d) DCCC from SAPHIR for the period June-August 2012 over the east Pacific Ocean.

3.1 Monthly mean position of ITCZ

Based on the analysis of the OFD, the monthly mean position of ITCZ is investigated in selected regions over the tropics between 25ºN and 25ºS (listed in Table I). Figure 6 shows the monthly mean zonal distribution of OFD over (a) West Pacific Ocean (b) Central Pacific Ocean (c) East Pacific Ocean (d) Atlantic Ocean (e) Indian Ocean (f) America (g) Africa and the (h) entire tropics for a normal year (2013, non-El-Niño year). Over the west Pacific Ocean, the ITCZ shows a broadband structure, migrating up to 20ºS during January. ITCZ starts migrating towards NH during May with OFD ranging between 1.2-1.8%. The peak OFD contours start migrating towards the SH by October. The ITCZ shows a narrow-band structure over the Central Pacific Ocean (CPO) with a prominent band of cloudiness around 5ºN - 10ºN. The SPCZ starts appearing during October, strengthens during January-April, and weakens by May over 10ºS - 20ºS at the central Pacific Ocean. Over the east Pacific Ocean (EPO), ITCZ is north of the equator throughout the year, migrating up to 20ºN during June-September. A weak

Table 1. Regions selected for the analysis of the strength and variability of ITCZ using DCCCs.

Region	Longitude
West Pacific Ocean (WPO)	120ºE to 160ºE
Central Pacific Ocean (CPO)	160ºE to 140ºW
East Pacific Ocean (EPO)	140ºW to 80ºW
Atlantic Ocean (AO)	30ºW to 10ºW
Indian Ocean (IO)	60ºE to 95ºE
America	75ºW to 50ºE
Africa	75ºW to 50ºE

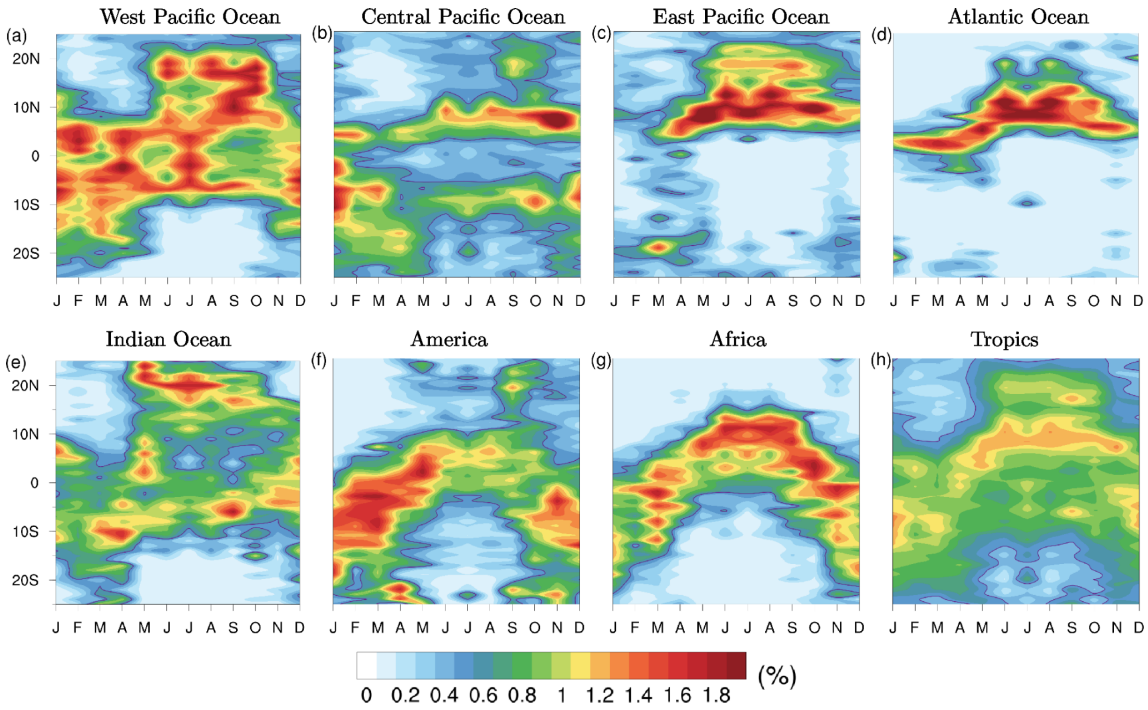

Figure 6. Monthly mean zonal distribution of occurrence frequency of DCCC over (a) West Pacific Ocean, (b) Central Pacific Ocean, (c) East Pacific Ocean, (d) the Atlantic Ocean, (e) the Indian Ocean, (f) America, (g) Africa, and (h) tropics.

ITCZ (OFD < 0.5%) is seen in the southern hemisphere in addition to northern hemispheric ITCZ during March and April months and weakens by May over the EPO. The dITCZ starts building up by the end of February, becomes prominent during March and April, and weakens by May. Over the Indian Ocean (IO), ITCZ exhibits a broadband structure. The dITCZ structure appears during November-February and April-May. The ITCZ over the Indian region migrates up to 20^{o}N during boreal summer resulting in heavy rainfall associated with the south Asian summer monsoon. The migration of ITCZ over the land regions of America and Africa is evident in Figures 6 (f) and 6 (g), respectively. Over the African landmass, the ITCZ migrates up to 15^{o}N in summer. The ITCZ crosses the equator twice a year over both regions. The migration of ITCZ is more prominent in Africa than in America. The ITCZ is mostly south of the equator during January, crosses the equator during March, and returns to the southern hemisphere by October over Africa. The global mean position of ITCZ is mostly south of the equator from November to April and North of the equator from May to October.

4. Conclusion

In the present study, ITCZ is identified and characterized using the brightness temperature of the SAPHIR payload aboard the Megha-Tropiques satellite from December 2011-November 2018. In this method, deep convective cloud cores where large upscale growth of the cloud occurs alone are identified, excluding the associated cirrus anvils. OFD with a threshold of 0.2% appears to be a better indicator of ITCZ. Results suggest that ITCZ identified using this approach has an added advantage over conventionally used parameters such as low OLR, high precipitation and near-surface wind convergence. OFD based ITCZ identification is free from the issues such as the contamination of OLR data by cold non-precipitating cirrus clouds, misinterpretation of heavy orographic precipitation as ITCZ by satellite rainfall data and the unavailability of surface wind data over land regions. The spatial pattern of ITCZ derived using the occurrence of DCCC is in good agreement with the surface wind convergence over the global oceans derived from satellite scatterometer observations. The mean position of ITCZ at every longitude is defined as the maximum time-mean OFD that lies within the region with SWC below the threshold of $-0.1\times10^{-5}s^{-1}$.

The monthly mean position and interannual variability of ITCZ over different regions of the tropics are analyzed using OFD. Globally, the mean position of the ITCZ is north of the equator extending as north as 24^{o}N over the Asian summer monsoon region during JJA. The ITCZ migrates up to 20^{o}S during DJF over the IO and WPO. It has a broad structure over WPO and IO. The ITCZ has a narrow-band structure over the CPO, EPO, and the Atlantic Ocean. The strength of ITCZ is predominant during La-Niña years over WPO. ITCZ shows interannual variations associated with El-Niño. During the El-Niño years, the double band structure of ITCZ merges and forms a single band, and the intensity of precipitation and OFD become more than twice the normal years over EPO and CPO. Over the EPO, ITCZ lies between 0^{o}and 10^{o}N throughout the year. The dITCZ structure is prominent during MAM. The OFD has increased to 1.8%, with a southward migration of ITCZ by 1^{o}- 2^{o}S latitudes during the El-Niño years. Over the equatorial Indian Ocean, ITCZ is found around 5^{o}S-10^{o}S with OFD of 0.8 - 1.2% during DJF. ITCZ starts migrating to the NH during JJA due to the onset of the summer monsoon.

Over Africa, maximum OFD reaches up to 1.4% with prominent seasonal migration extending up to 10^{o}S during MAM to 15^{o}N during JJA. ITCZ is mainly located south of the equator over the American landmass, with OFD and precipitation reduced considerably during the El-Niño years. Africa and America show prominent seasonal migration of ITCZ and cross the equator twice a year during March and October. The monthly mean OFD over seven selected regions are analyzed to study the long-term variability in the strength of ITCZ. No significant trend is seen over the tropics during the study period (2011-2018). The ITCZ captured by OFD is sharper and narrower than the ITCZ captured by other parameters and is a better proxy over land. The present study examined the mean position and migration of ITCZ using DCCCs derived from a passive microwave sounder aboard the low-inclination Megha-Tropiques satellite for the first time. Low-orbital inclination satellites similar to Megha-Tropiques, with the primary objective of repeated measurements of water vapour and energy budget parameters at different local times, are of high demand to the scientific community for data continuity.

6. Acknowledgements

The authors would like to thank Dr. K. Rajeev, Director, Space Physics Laboratory, VSSC, Thiruvananthapuram for the fruitful discussions. The SAPHIR and ScaRaB data aboard MT is obtained from MOSDAC (www.mosdac.gov.in). MODIS monthly mean SST, TRMM monthly mean precipitation and ASCAT wind products were obtained from podaac-tools.jpl.nasa.gov. The CloudSat geometrical profile (2B-GEOPROF) product, which contains radar reflectivity data utilizing algorithms to identify the vertical profile of the cloud system was obtained from www.cloudsat.cira.colostate.edu. Sisma Samuel is a research student registered for Ph.D. at Cochin University of Science and Technology and acknowledges ISRO Research Fellowship.

7. References

[1] S. Nicholson, “The ITCZ and the seasonal cycle over equatorial Africa,” Bulletin American Meteorological Society, vol.99, pp. 337–348, 02 2018, 10.1175/BAMS-D-16-0287.1.

[2] D. E. Waliser and C. Gautier, “A satellite-derived climatology of the ITCZ,” J. of Climate, vol. 9, pp. 2958–2972, 1995, 10.1175/1520-0442(1993)006.

[3] S. G. H. Philander, D. Gu, G. Lambert, T. Li, D. Halpern, N.-C. Lau, and R. C. Pacanowski, “Why the ITCZ is mostly north of the equator?” J. of Climate, vol. 9, no. 12, pp. 2958–2972, 1996, 10.1175/1520-0442.

[4] U. Nedjeljka, G. Skok, and J. Tribbia, “Climatology of the ITCZ derived from ERA Interim reanalyses,” J. Geophysical. Research. :Atmosphere, vol. 116, 08 2011.

[5] T. Schneider, T. Bischoff, and G. Haug, “Migrations and dynamics of the Intertropical Convergence Zone,” Nature, vol. 513, pp.45–53, 09 2014, 10.1038/nature13636.

[6] M. Byrne and T. Schneider, “Energetic constraints on the width of the Intertropical Convergence Zone,” J. of Climate, vol. 29, pp.4709–4721, 07 2016, 10.1175/JCLI-D-15-0767.1.

[7] E. Castelli, E. Papandrea, M. Valeri, F. P. Greco, M. Ventrucci, S. Casadio, and B. M. Dinelli, “ITCZ trend analysis via Geodesic P-spline smoothing of the AIRWAVE TCWV and cloud frequency datasets,” Atmospheric Research, vol. 214, pp. 228–238, 2018.

[8] C. Liu, X. Liao, J. Qiu, Y. Yang, X. Feng, R. P. Allan, N. Cao, J. Long, and J. Xu, “Observed variability of intertropical convergence zone over 1998—2018,” Environmental Research Letters, vol. 15, no. 10, p. 104011, sep 2020.

[9] S. C. Sherwood and A. E. Dessler, “A model for transport across the tropical tropopause,” J. of Atmospheric Science, vol. 58, no. 7, pp. 765–779, 2001, 10.1175/1520-0469(2001).

[10] A. Gettelman, M. L. Salby, and F. Sassi, “Distribution and influence of convection in the tropical tropopause region,” J. Geophysical. Research. :Atmosphere, vol. 107, no. 4, 2002.

[11] J. T. Kiehl, K. E. Trenberth, and J. T. Fasullo, “Earth's global energy budget,” Bulletin American Meteorological Society, March 2009.

[12] R. Pierrehumbert, “Thermostats, radiator fins, and the local runaway greenhouse,” J. of Atmospheric Science, vol. 52, pp. 1784–1806, 05 1995, 10.1175/1520-0469(1995)052.

[13] S. Bony, B. Stevens, D. Coppin, T. Becker, K. Reed, A. Voigt, and B. Medeiros, “Thermodynamic control of anvil cloud amount,”Proceedings of the National Academy of Sciences, vol. 113, p. 201601472, 07 2016, 10.1073/pnas.1601472113.

[14] H. Su, J. Neelin, T. Shen, C. Zhai, Q. Yue, Z. Wang, L. Huang, Y.-S. Choi, G. Stephens, and Y. Yung, “Tightening of tropical ascent and high clouds key to precipitation change in a warmer climate,” Nature Communications, vol. 8, 06 2017, 10.1038/ncomms15771.

[15] S. Gadgil and A. Guruprasad, “An objective method for the identification of the Intertropical Convergence Zone,” J. of Climate,vol. 3, 05 1990, 10.1175/1520-0442(1990)003.

[16] C. E. Lietzke, C. Deser, and T. H. V. Haar, “Evolutionary structure of the eastern pacific double (ITCZ) based on satellite moisture profile retrievals,” J. of Climate, vol. 14, no. 4, pp. 743–751, 2001.

[17] G. Gu and C. Zhang, “Cloud components of the Intertropical Convergence Zone,” J. Geophysical. Research. :Atmosphere, vol.107, no. D21, 2002, 10.1029/2002JD002089.

[18] W. T. Liu and X. Xie, “Double Intertropical Convergence Zonesa new look using scatterometer,” Geophysical Research Letters,vol. 29, no. 22, pp. 29–1–29–4, 2002, 10.1029/2002GL015431.

[19] T. Schneider and T. Bischoff, “Energetic constraints on the position of the Intertropical Convergence Zone,” J. of Climate, vol. 27, pp. 4937–4951, 06 2014, 10.1175/JCLI-D-13-00650.1.

[20] T. Bischoff and T. Schneider, “The equatorial energy balance, ITCZ position, and double ITCZ bifurcations,” J. of Climate, vol. 29, p. 151023105856005, 10 2015, 10.1175/JCLI-D-15-0328.1.

[21] J. Shonk, E. Guilyardi, T. Toniazzo, S. Woolnough, and T. Stockdale, “Identifying causes of western Pacific ITCZ drift in ECMWF System 4 hindcasts,” Climate Dynamics, vol. 50, pp. 1–16, 02 2018, 10.1007/s00382-017-3650-9.

[22] G. Zhang, S. Xiaoliang, and W. Yong, “The double ITCZ syndrome in GCMs: A coupled feedback problem among convection, clouds, atmospheric and ocean circulations,” Atmospheric Research, vol. 229, 06 2019, 10.1016/j.atmosres.2019.06.023.

[23] B. Tian and X. Dong, “The Double-ITCZ bias in CMIP3, CMIP5 and CMIP6 models based on annual mean precipitation,” Geophysical Research Letters, vol. 47, p. e2020GL087232, 03 2020, 10.1029/2020GL087232.

[24] B. A. Burns, X. Wu, and G. R. Diak, “Effects of precipitation and cloud ice on brightness temperatures in AMSU moisture channels,” IEEE Trans. Geosci. Remote Sens., vol. 35, no. 6, pp. 1429–1439, 1997.

[25] G. Hong, G. Heygster, J. Miao, and K. Kunzi, “Detection of tropical deep convective clouds from AMSU-B water vapor channels measurements,” J. Geophysical. Research. :Atmosphere, vol. 110, no. 4, 2005.

[26] N. Mathew, C. Suresh Raju, R. Renju, and T. Antony, “Distribution of tropical deep convective clouds from Megha-Tropiques SAPHIR data,” IEEE Trans. Geosci. Rem. Sens., pp. 6409–6414, 2016.

[27] S. Samuel, N. Mathew, M. Kumar, and R. Renju, “Spatial and temporal variability of deep convective clouds over the tropics using multi-year Megha-Tropiques-Sondeur Atmosphérique duProfil d’Humidité Intertropicale par Radiométrie (SAPHIR) observations,” International J. of Remote Sensing, vol. 43, 2021, 10.1080/01431161.2021.1910368.

[28] G. Raju, “Engineering challenges in the Megha-Tropiques satellite,” Current Science, vol. 104, no. 12, 2013.
[29] S. Samuel, N. Mathew, and V. Sathiyamoorthy, “Association of the occurrence of deep convective cloud cores with sea surface temperatures over the equatorial Indian and the western Pacific oceans,” Atmospheric Research, p. 106034, 2022
[30] P. Liu, L. Chongyin, W. Yu, and F. Yunfei, “Climatic characteristics of convective and stratiform precipitation over the tropical and subtropical areas as derived from TRMM PR,” Science China Earth Sciences, vol. 56, 03 2012.
[31] G. L. Stephens, et al., and The CloudSat team, “The CLOUDSAT Mission and the A-train. A New Dimension of Space-Based Observations of Clouds and Precipitation,” Bulletin of the American Meteorological Society, vol. 83, no. 12, pp. 1771–1790, December 2002.
[32] B. Utsav, S. M. Deshpande, S. K. Das, G. Pandithurai, and D. Niyogi, “Observed vertical structure of convection during dry and wet summer monsoon epochs over the Western Ghats,” J. Geophysical. Research. :Atmosphere, vol. 124, no. 3, pp. 1352–1369, 2019.